ISSN 0022-4766, Journal of Structural Chemistry, 2022, Vol. 63, No. 8, pp. 1262-1273. © Pleiades Publishing, Ltd., 2022.
Text © The Author(s), 2022, published in Zhurnal Strukturnoi Khimii, 2022, Vol. 63, No. 8, 96112.

AN INVESTIGATION INTO THE IMPACT OF INTRODUCED THIOCYANATE ANIONS ON THE TRINUCLEAR Co(II) SALAMO-BASED COMPLEX

K.-F. Xie[1], Y. Huang[1], S.-Z. Li[1], L.-L. Li[1], and W.-K. Dong[1]*

The reaction of $Co(OAc)_2 \cdot 4H_2O$ with multisite coordinated salamo-based ligand H_2L containning six coordinating sites in presence of co-ligand NCS^- anions afforded successfully a trinuclear Co(II) complex $[Co_3(L)_2(NCS)_2]$. The trinuclear Co(II) complex has been characterized by elemental analyses, UV-Vis, Fourier transform infrared spectroscopic methods and DFT calculation. In addition, the structure of the Co(II) complex has been confirmed by single crystal X-ray crystallography. X-ray crystal structure analysis of the Co(II) complex revealed that the Co(II) complex consists of three Co(II) atoms coordinated by two fully deprotonated ligand $(L)^{2-}$ units and co-ligand NCS^- anions. The close surveillance of the crystal structure of the Co(II) complex discloses some notable non-covalent interactions like H-bonding, C-H···π and π···π. The luminescent property of the Co(II) complex has been studied in methanol solution. Apart from, as a complementary revelation, intermolecular interactions with respect to percentages of hydrogen bondings in the X-ray crystal structure of the trinuclear Co(II) complex was quantified by analyses of Hirshfeld surfaces and fingerprint plots.

DOI: 10.1134/S0022476622080078

Keywords: salamo-based ligand, Co(II) complex, crystal structure, Hirshfeld surface, luminescence property.

INTRODUCTION

Recently, transition metal ions [1, 2] have attracted considerable attention because of their interesting molecular structures when prepared in conjunction with co-ligands [3, 4]. Moreover, multinuclear metal complexes also are of continual interest of the chemists because their functionalities, connectivity, porosities and structural variations make them promising materials for applications in the field of magnetism, materials, biology sensors, and catalysis [5-10].

Generally, the common strategy of synthesizing multinuclear transition metal complexes is completed by appropriate organic ligands, bridging anions and co-ligands. However, the structure and nuclearity of these types of complexes are affected by various factors, such as charge, coordination number and geometry of metal ion, shape and size of ligands, flexibility, denticity and HSAB behavior.

In this context, salen-based ligands can serve as a better candidate to construct the architects of multinuclear transition metal complexes. However, among the derivatives of salen-based ligands, salamo-based ligands exploited firstly by

[1]School of Chemistry and Chemical Engineering, Lanzhou Jiaotong University, People′s Republic of China; *dongwk@126.com. Original article submitted February 6, 2022; revised March 10, 2022; accepted March 21, 2022.

Nabeshima group [11] are more excellent candidates. This is because salamo-based ligands introduce strong electronegative oxygen atoms into the C=N group of salen-based ligands, which makes the chemical properties of salamo-based ligands more stable than salen-based ligands [12-14]. A great variety of salamo-based ligands have been used to synthesize not only structurally different but also quite interesting mononuclear [15], polynuclear [16] and heteropolynuclear metal complexes [17]. The above complexes were found to possess wide applications in the field of catalysis [18-20], electron transport processes [21], organic catalysis, bioinorganic chemistry [10], luminescent properties [22], molecular recognitions [12] and magnetism [23]. Thiocyanate anion (SCN^-) is well known flexidentate co-ligand that is simultaneously coordinate with transition metal ions in versatile coordination modes [24-27]. Therefore, the combination of salamo-based ligands with multiple coordination sites and flexidentate co-ligand creates conditions for the synthesis of structurally novel complexes with diverse structures.

In the present work, a trinuclear Co(II) complex $[Co_3(L)_2(NCS)_2]$ was successfully synthesized by using a salamo-based ligand H_2L with multiple coordination sites. The Co(II) complex was characterized by single crystal X-ray diffraction. The luminescent property of the Co(II) complex was studied. In addition, investigation of Hirshfeld surfaces and 2D finger print plots was devoted to analyze carefully non-covalent supramolecular interactions.

EXPERIMENTAL

Materials and general methods. 3-Methoxysalicylaldehyde (99%) was purchased from Alfa Aesar. The solvents required for other experiments were purchased from Tianjin Chemical Reagent Factory. Use the GmbH VarioEL V3.00 automatic element analyzer for C, H and N analysis. Elemental analysis of Co(II) was performed using IRIS ER/S·WP-1 ICP atomic emission spectrometer. The ^{1}H NMR spectra were measured on a Bruker AV 500 MHz spectrometer. The melting points were measured by a micro melting point instrument manufactured by Beijing Tektronix Instrument Co., Ltd. FTIR spectra were conducted by KBr (500-4000 cm^{-1}) and CsI (100-500 cm^{-1}) pellets on a VERTEX70 FTIR spectrophotometer (Bruker, Billerica, MA, USA). UV-Vis absorption and fluorescence spectra were determined using Shimadzu UV-3900 (Shimadzu, Japan) and Hitachi F-7000 (Hitachi, Tokyo, Japan) spectrometers, respectively. The 1 cm quartz cuvette and Xe lamp were used as light source to record the fluorescence spectra. The X-ray single crystal structure was measured on a Bruker Smart Apex CCD diffractometer. Hirshfeld surface analysis of the Co(II) complex was performed using the Crystal Explorer program were all made according to similar methods previously reported.

Crystallographic data collection and refinement. X-ray diffraction data of the Co(II) complex was collected on a Bruker D8 Venture diffractometer with the graphite-monochromatized CuK_α (λ = 0.71073 Å) radiation. The complex cooled in a nitrogen gas cryostream to 173 K. Data collection was performed with the APEX2 software package and data reduction was performed using the SAINT V8.38A programs [28]. The multiscan program SADABS [29] was used for absorption correction. The coordinates of the non-hydrogen atoms were refined anisotropically, whereas hydrogen atoms were included in the calculation isotropically but not refined. The crystal structure of the Co(II) complex was solved by the direct method and refined by the full-matrix least-squares method used the SHELXL2018/3 programs implemented in Olex2 program [30]. Selected data of parameters and refinement of the Co(II) complex are summarized in Table 1.

Synthesis of H_2L. The salamo-based ligand H_2L was synthesized by following reported method [31]. H_2L is a multisite coordination ligand that contains six coordinating sites in the form of two phenolic oxygen atoms, two oxime nitrogen atoms and two methoxy oxygen atoms. Yield 79% (571.2 mg). Found (%): C 60.16, H 5.38, N 7.55. $C_{18}H_{20}N_2O_6$. Calculated (%): C 59.99, H 5.59, N 7.77. ^{1}H NMR (500 MHz, $CDCl_3$): δ, ppm 9.73 (s, 1H), 8.26 (s, 1H), 6.91(dd, *J* = 7.8 Hz, 1.7 Hz, 1H), 6.85 (t, *J* = 7.8 Hz, 1H), 6.82 (dd, *J* = 7.8 Hz, 1.8 Hz, 1H), 4.48 (s, 4H), 3.91 (s, 6H).

Synthesis of the Co(II) complex. The synthetic route of the Co(II) complex is shown in Scheme 1. A methanol solution (3 mL) of $Co(OAc)_2{\cdot}4H_2O$ (1.5 mmol, 2.86 mg) was added to the acetonitrile solution (1 mL) of the ligand H_2L (1 mmol, 3.62 mg) with constant stirring. Then a methanol solution (1 mL) of potassium thiocyanate (1 mmol, 1.00 mg) was added to the mixture. Finally, add a little triethylamine to the mixed solution, and the color of the solution changes from

TABLE 1. Crystallographic Data and Refinement Parameters for the Co(II) Complex

Parameter	The Co(II) complex
Empirical formula	$C_{38}H_{36}Co_3N_6O_{12}S_2$
Formula weight	1009.64
Temperature, K	173.0
Wavelength, Å	0.71073
Crystal system	Monoclinic
Space group	$P2_1/n$
Unit cell dimension: a, b, c, Å; β, deg	22.0383(8), 9.4323(4), 22.2733(8); 117.067(2)
V, Å^3	4122.9(3)
Z	4
D_{calc}, g/cm^3	1.627
μ, mm^{-1}	10.892
F(000)	2060.0
Crystal size, mm	0.12×0.11×0.09
θ range, deg	4.676 to 136.4
Index ranges	$-26 \le h \le 26$, $-17 \le k \le 17$, $-20 \le l \le 20$
	$-10 \le k \le 11$, $-26 \le l \le 26$
Reflections collected / independent	27159 / 7499
Completeness to % θ, deg	99.5
Data / restraints / parameters	7499 / 0 / 555
Final R_1, wR_2 indices ($I > 2\sigma(I)$)	0.0559, 0.1116
$GOOF$	0.963
$\Delta\rho_{max}$ / $\Delta\rho_{min}$, e/Å^3	0.37 / –0.49

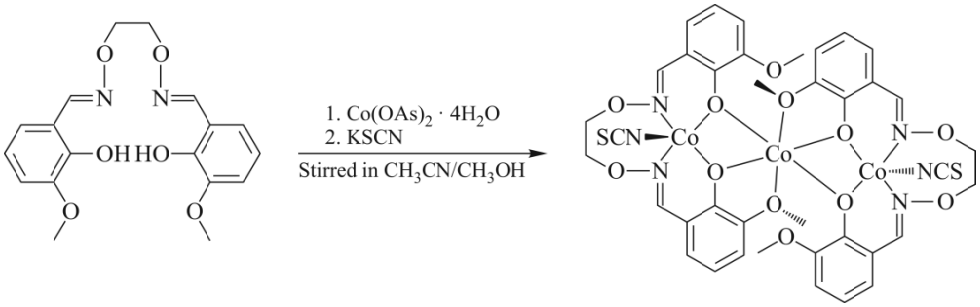

Scheme 1. Synthesis of the Co(II) complex.

yellow to brown instantly. The resulting solution was stirred further for 30 min. The brown solution was then filtered and kept in a vial at room temperature. Dark brown block-shaped single crystals were then collected after several weeks. Yield: 38% (1.92 mg). Found (%): C 47.19, H 3.32, Co 17.37, N 8.21. $[Co_3(L)_2(NCS)_2]$ ($C_{38}H_{36}Co_3N_6O_{12}S_2$). Calculated (%): C 45.21, H 3.59, Co 17.51, N 8.32.

RESULTS AND DISCUSSION

IR spectra. The IR spectrum of the Co(II) complex was analyzed and systematically compared with that of the corresponding free ligand H_2L in the 4000-400 cm^{-1} region (Fig. 1). In the IR spectrum of the ligand, the appearance of a broad band around 3167 cm^{-1} indicates the presence of O–H stretching vibration [32-34] of phenolic hydroxyl group of the free ligand H_2L. In present case, a strong absorption band at about 1606 cm^{-1} in the IR spectrum of the Co(II) complex was

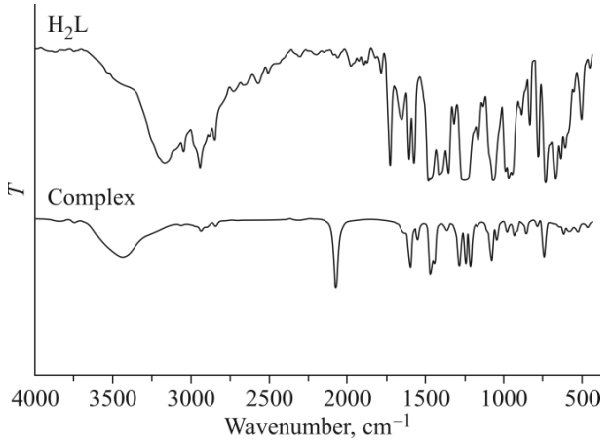

Fig. 1. The IR spectra of H_2L and its corresponding Co(II) complex.

observed which are attributed to ν(C=N) stretching frequency [35, 36]. An intense band near at 1598 cm^{-1} for the Co(II) complex is shifted to a lower energy value compared to that of H_2L, which further confirms coordination binding mode of the oxime nitrogen atoms with the Co(II) centers. In addition, a characteristic Ar–O stretching frequency for H_2L was observed at about 1260 cm^{-1}, while that of the Co(II) complex appeared at about 1247 cm^{-1}. The appearance of a strong absorption band ν(C≡N) around 2071 cm^{-1}, a weak absorption peak ν(C≡S) at 845 cm^{-1} and a weak absorption peak δ_{NCS} at 461 in the IR spectrum of the Co(II) complex clearly indicates the presence of NCS^- anions with N as the coordination atoms [3, 37], which is also evident from the crystal structure determination.

Further, the far-infrared spectrum of the Co(II) complex in the range of 500-100 cm^{-1} was also obtained so as to identify the bonds of Co–O and Co–N frequencies. The band at around 461 cm^{-1} in the Co(II) complex can be attributed to ν_{Co-O}, while the band at 528 cm^{-1} is assigned to ν_{Co-N} [16].

UV–Vis absorption spectral analyses. The UV-Vis spectra of H_2L and its Co(II) complex were measured in methanol solution ($1 \cdot 10^{-5}$ mol/L) at room temperature. (Fig. 2*a*).

The free ligand exhibits intense absorption bands at approximately 227 nm and 271 nm in the UV region which are presumably due to the π–π* type transitions of the aromatic rings, whereas the free ligand displays intense absorption band at 316 nm presumably attributed to the π–π* transitions of C=N bonds [38]. It is clear that the corresponding absorption band of the Co(II) complex has bathochromically shifted to approximately 234 nm, 273 nm and 341 nm, respectively, which may be

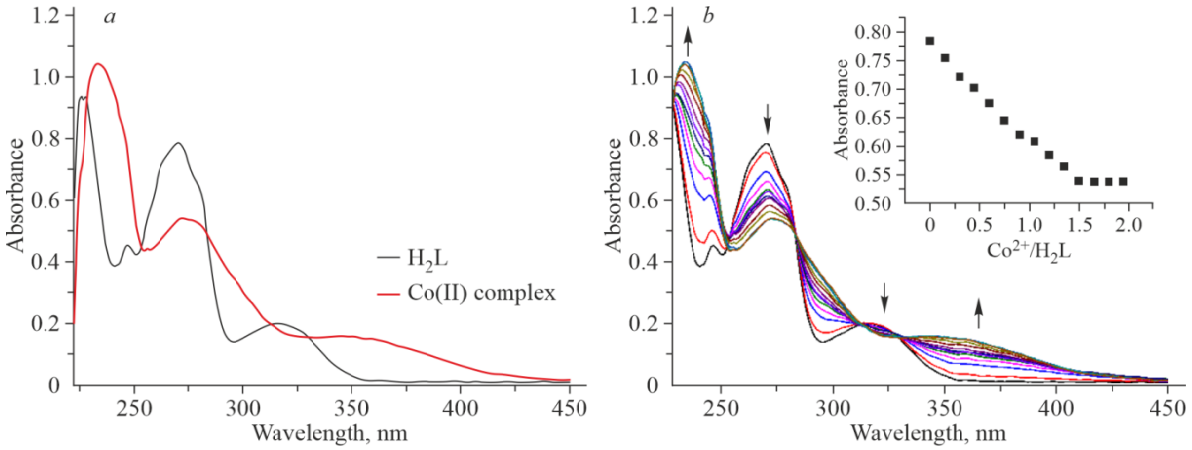

Fig. 2. UV-Vis spectra of H_2L and its Co(II) complex (nm) (*a*), UV-Vis spectra of H_2L with increasing concentrations of $Co(OAc)_2 \cdot 4H_2O$ in methanol (*b*).

due to the structural environment of H_2L and the perturbation of the intra-ligand π–π* transition by the Co(II) ions which are nearly comparable with previously reported Co(II) complexes [20].

To examine formation reaction of the Co(II) complex, there executed UV-Vis titration in the range of 220-450 nm by the gradual addition of $1 \cdot 10^{-3}$ mol/L methanol solution of $Co(OAc)_2 \cdot 4H_2O$ to a $1 \cdot 10^{-5}$ mol/L methanol solution (2 mL) of H_2L (Fig. 2*b*).

The absorption intensities of the bands of H_2L at 271 nm and 316 nm kept on decreased, while new absorption band centered at approximately 341 nm appeared with increasing intensity with an increase in the concentration of $Co(OAc)_2 \cdot 4H_2O$ is shown in Fig. 2*b*. Furthermore, three isosbestic points were found at approximately 254 nm, 312 nm and 331 nm in the UV-Vis titration spectra, which indicated that an equilibrium between H_2L, $Co(OAc)_2 \cdot 4H_2O$ and the Co(II) complex in the solution was reached. When H_2L and Co^{2+} ions concentration ratio reached 2:3, the titration reached the end point [20]. This implied a 2:3 (H_2L:Co^{2+}) type complex formed which is also confirmed from single crystal X-ray structure.

Crystal structure of the Co(II) complex. The X-ray crystal structure determination revealed that the Co(II) complex crystallizes in the monoclinic space group $P2_1/c$. The Co(II) complex consists of three Co(II) atoms which was assembled with the support of two fully deprotonated ligand $(L)^{2-}$ units and co-ligand NCS^- anions (Fig. 3). In addition, it can be clearly found that the OAc^- anion is not involved in coordination from the X-ray crystal structure of the Co(II) complex, which is different from the common structures of the trinuclear cobalt(II) complexes reported previously [39]. Table 2 provides the main bond parameters of the Co(II) complex.

Notably, both of the terminal Co1 and Co3 atoms in the Co(II) complex are penta-coordinate and not hexa-coordinate as common Co(II) complexes as previously reported [39], whose coordination geometry is completed by two oxime nitrogen atoms (Co1: N1 and N2, Co3: N4 and N5) and two phenoxo oxygen atoms (Co1: O1 and O5, Co3: O11 and O7) from the fully deprotonated ligand $(L)^{2-}$ units, while the apical position is occupied by one nitrogen atom (Co1:N3, Co3:N6) from isothiocyanate anions. The Addison parameter τ_{Co1} and τ_{Co3} ($\tau = (\beta - \alpha)/60$, β and α are the largest angle and the second largest angle, respectively.) for the penta-coordinated Co1 and Co3 atoms are 0.59 and 0.68, respectively, indicating the geometries are significantly distorted trigonal bipyramidal [40]. At the same time, the axial bond length also well confirms this result, and the bond length parameters are shown in Table 1. The center Co2 atom is hexa-coordinated, whose coordination geometry is completed by six O atoms (O1, O5, O2, O11, O7 and O12) from the two fully deprotonated ligand $(L)^{2-}$ units in which one of the two methoxy O atoms in the ligand $(L)^{2-}$ unit is not coordinated. The Co2 atom has a distorted octahedral geometry.

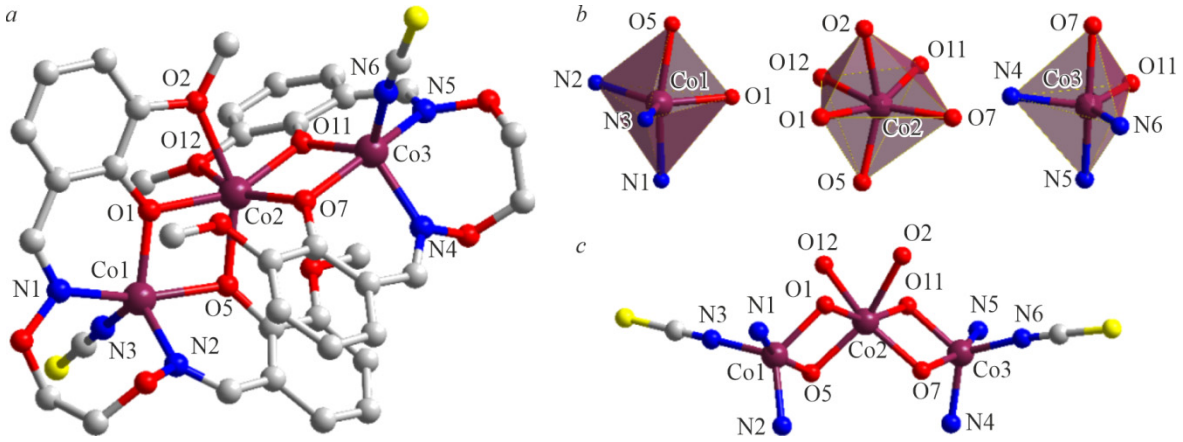

Fig. 3. Representation of the X-ray crystal structure of the Co(II) complex. (Hydrogen atoms have been omitted for clarity) (*a*); coordination configurations for Co(II) atoms of the Co(II) complex (*b*); perspective view of only Co(II) atoms with coordinating atoms, the coordinated co-ligand NCS^- anions are shown for clarity (*c*).

TABLE 2. The Main Bond Distances and Angles in the Co(II) Complex

Bond length	Distance, Å	Bond length	Distance, Å	Bond length	Distance, Å
Co1–O1	1.951(5)	Co2–O5	2.058(5)	Co3–N4	2.008(6)
Co1–N3	1.979(5)	Co2–O1	2.012(4)	Co3–O7	2.098(5)
Co1–O5	2.085(4)	Co2–O11	2.014(5)	Co3–O11	1.949(4)
Co1–N1	2.100(6)	Co2–O2	2.278(5)	Co3–N5	2.112(7)
Co1–N2	2.001(6)	Co2–O12	2.240(4)	Co3–N6	1.961(6)
		Co2–O7	2.050(4)		
Bond angle	**Value, deg**	**Bond angle**	**Value, deg**	**Bond angle**	**Value, deg**
O1–Co1–O5	78.23(17)	O5–Co2–O12	94.70(16)	O11–Co2–O12	74.67(17)
O1–Co1–N3	116.7(2)	O1–Co2–O2	73.75(17)	O7–Co3–N5	162.6(2)
O5–Co1–N3	96.0(2)	O1–Co2–O11	154.83(18)	O11–Co3–N5	86.9(2)
N2–Co1–N3	113.9(3)	O2–Co2–O7	98.33(16)	N4–Co3–N6	115.3(2)
O1–Co1–N1	87.8(2)	O5–Co2–O7	95.65(17)	N5–Co3–N6	100.1(3)
O5–Co1–N1	163.3(2)	O7–Co2–O11	78.09(17)	O7–Co3–N6	95.6(2)
N1–Co1–N2	95.6(2)	O1–Co2–O7	118.64(17)	O11–Co3–N6	121.4(2)
O1–Co1–N2	128.2(2)	O2–Co2–O11	85.78(17)	N4–Co3–N5	94.2(2)
N1–Co1–N3	98.4(2)	O5–Co2–O11	121.76(17)	O7–Co3–O11	78.38(17)
O5–Co1–N2	86.2(2)	O1–Co2–O12	88.62(16)	O7–Co3–N4	85.9(2)
O2–Co2–O5	151.27(17)	O1–Co2–O5	77.52(17)	O11–Co3–N4	122.1(2)
O2–Co2–O12	84.32(16)	O7–Co2–O12	152.36(18)		

A detailed examination of the crystal structure of the Co(II) complex disclosed the presence of extensive C–H···π, π···π stacking and hydrogen bond interactions.

Fig. 4*a* shows two linking complexes which is formed due to a pair of the significant C–H···π (C29–H29B–*Cg*11) interactions. The hydrogen atom H29B attached to carbon atom C29 is involved in intermolecular C–H···π interaction with phenyl ring *Cg*11 (*Cg*11: C20–C21–C22–C23–C24–C25). The intramolecular C–H···π (C18–H18B–*Cg*12) and π···π (*Cg*10–*Cg*11) stacking interactions of the Co(II) complex were observed in Fig. 4*b*. The hydrogen atom H18B attached to carbon atom C18 is involved in intramolecular C–H···π interaction with phenyl ring *Cg*12 (*Cg*12: C31–C32–C33–C34–C35–C36). The π···π stacking interaction between the two neighboring aromatic rings (*Cg*10 and *Cg*11) was found with a centroid-to-centroid distance of 3.957(2) Å. The hydrogen atom H9A attached with C9 and H29A attached with C29 are also engaged in intramolecular hydrogen bond (Fig. 4*c*) with the nitrogen atoms N3 and N6 of NCS^- anions. Hydrogen bond distances and angles for the Co(II) complex are given in Table 3.

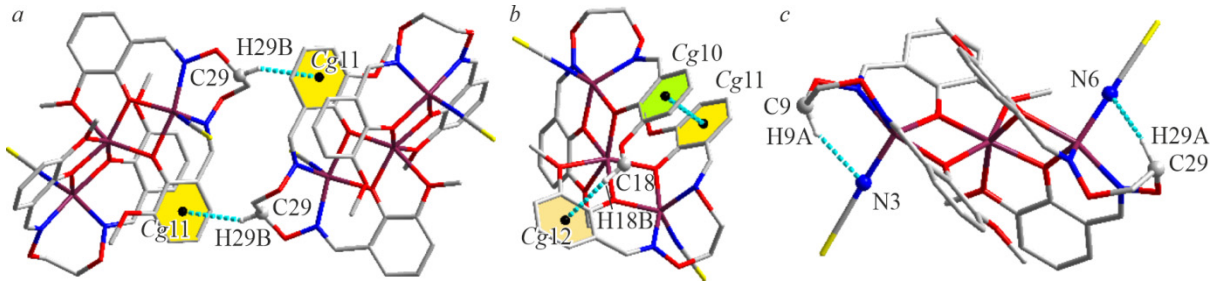

Fig. 4. The viewpoint of intermolecular C–H···π interactions of the Co(II) complex (*a*); the intramolecular C–H···π and π···π stacking interactions of the Co(II) complex (*b*); the viewpoint of intramolecular hydrogen bonds of the Co(II) complex (*c*).

TABLE 3. Hydrogen Bond Lengths and Angles in the Co(II) Complex

D–H···*A*	$d_{(D\text{-}H)}$, Å	$d_{(H\text{-}A)}$, Å	$d_{(D\text{-}A)}$, Å	∠(*DHA*), deg	Symmetry code
C9–H9A···N3	0.99	2.49	3.399(9)	152	
C11–H11···S1	0.95	2.83	3.689(7)	151	1/2–*x*, –1/2+*y*, 3/2–*z*
C26–H26···S2	0.95	2.82	3.687(6)	153	1–*x*, 1–*y*, 1–*z*
C29–H29A···N6	0.99	2.54	3.430(9)	149	
C35–H35···O10	0.95	2.60	3.420(9)	145	3/2–*x*, 1/2+*y*, 3/2–*z*

Luminescent properties. The emission spectral behaviors of the ligand H_2L and its corresponding Co(II) complex were studied at normal room temperature using MeOH solution in the range of 350-550 nm. The fluorescence spectra of the free ligand H_2L and its Co(II) complex are clearly represented in Fig. 5*a*.

Upon excitation wavelength at *ca* 330 nm, the free ligand H_2L demonstrated an intense fluorescent emission peak centered mainly at approximately 403 nm which should be assigned to the intra-ligand π–π* transition whereas the emission maxima for the Co(II) complex appeared at approximately 397 nm. Further a very careful investigation from emission spectral curves of H_2L and its Co(II) complex revealed that the Co(II) complex exhibits hypsochromically shifted with respect to the free ligand H_2L mainly assigned to the L → M charge transfer [41]. For such single salamo-based complexes, the crystal structure is basically the same as the solution structure, and there will be no dissociation [39, 42].

In addition, the fluorescence intensities of the Co(II) complex is about 4-fold lower compared to that of H_2L from the spectra, which probably may be due to N/O-donor centers coordination with the Co(II) atoms.

The fluorescence titration of H_2L ($1\cdot10^{-5}$ mol/L) in 2 mL methanol solution is carried out by the gradual addition of $Co(OAc)_2\cdot4H_2O$ ($1.0\cdot10^{-3}$ mol/L) (Fig. 5*b*). With the increase of Co^{2+} ion concentration, the fluorescence intensity of the Co(II) complex weaken linearly until quenching, and the emission peak has hypsochromically shifted as the fluorescence intensity weaken. It most probably due to the formation of the Co(II) complex after coordination *via* N,O-donor centers with Co(II) atoms [40].

Hirshfeld surface analysis. Supramolecular interactions of the Co(II) complex were investigated using Hirshfeld surface analysis. Calculations of Hirshfeld surfaces [43, 44] were performed using the CrystalExplorer (version 17.5) software package [45]. The Hirshfeld surfaces of the Co(II) complex mapped over curvedness, d_{norm} and shape index are illustrated in Fig. 6.

The C–H···O interactions represent the closest contacts in the structure and can be viewed as red spots on the d_{norm} surface and other visible spots on the surface correspond to H···H contacts. Furthermore, it is clear that the X-ray crystal

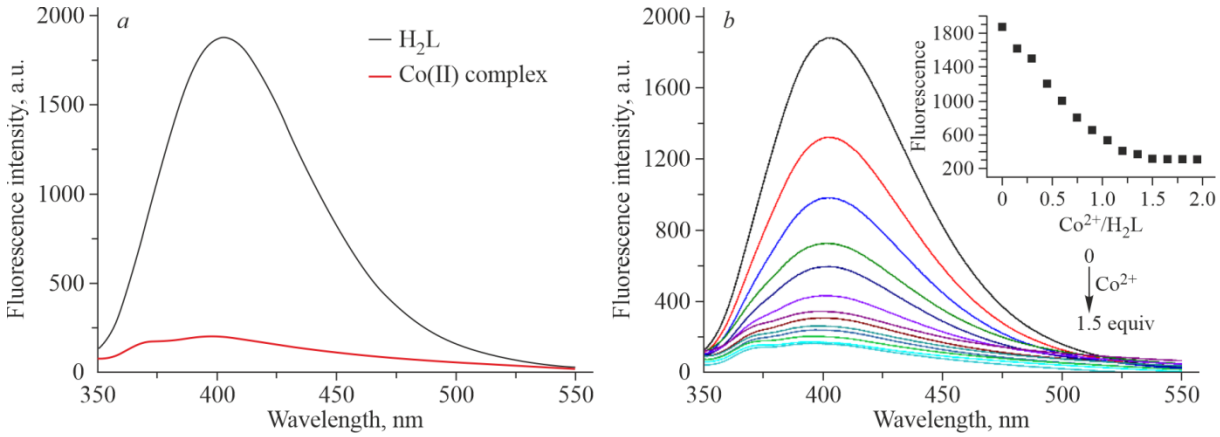

Fig. 5. Fluorescence spectra of H_2L and its corresponding Co(II) complex (*a*); fluorescence spectra of H_2L with increasing concentrations of $Co(OAc)_2\cdot4H_2O$ in methanol (*b*).

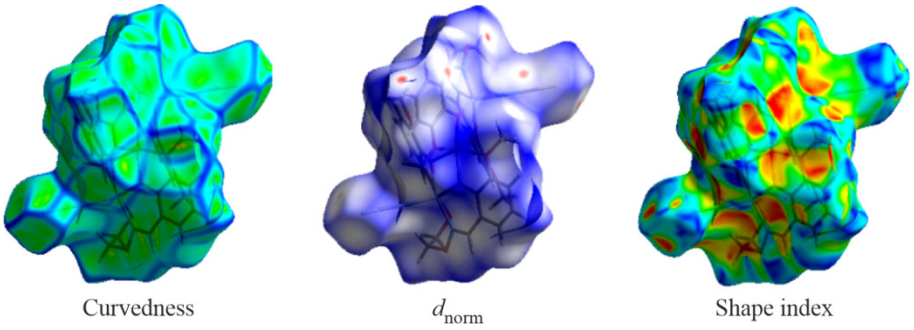

Fig. 6. Hirshfeld surfaces mapped with curvedness, d_{norm} and shape index of the Co(II) complex; the surfaces are shown as transparent to allow visualization of the orientation and conformation of the functional groups in the molecules.

structure of the Co(II) complex do not exhibit any intermolecular π···π stacking interaction since there is no evidence of the adjacent red and blue triangles on the shape index surfaces.

CrystalExplorer software package also was commonly used to construct fingerprint plots analysis [46] which employed successfully to illustrate intermolecular interaction patterns and the relative contributions. Fingerprint plots for the Co(II) complex and relevant surface patches associated with the specific contacts in the d_{norm} showed in Fig. 7.

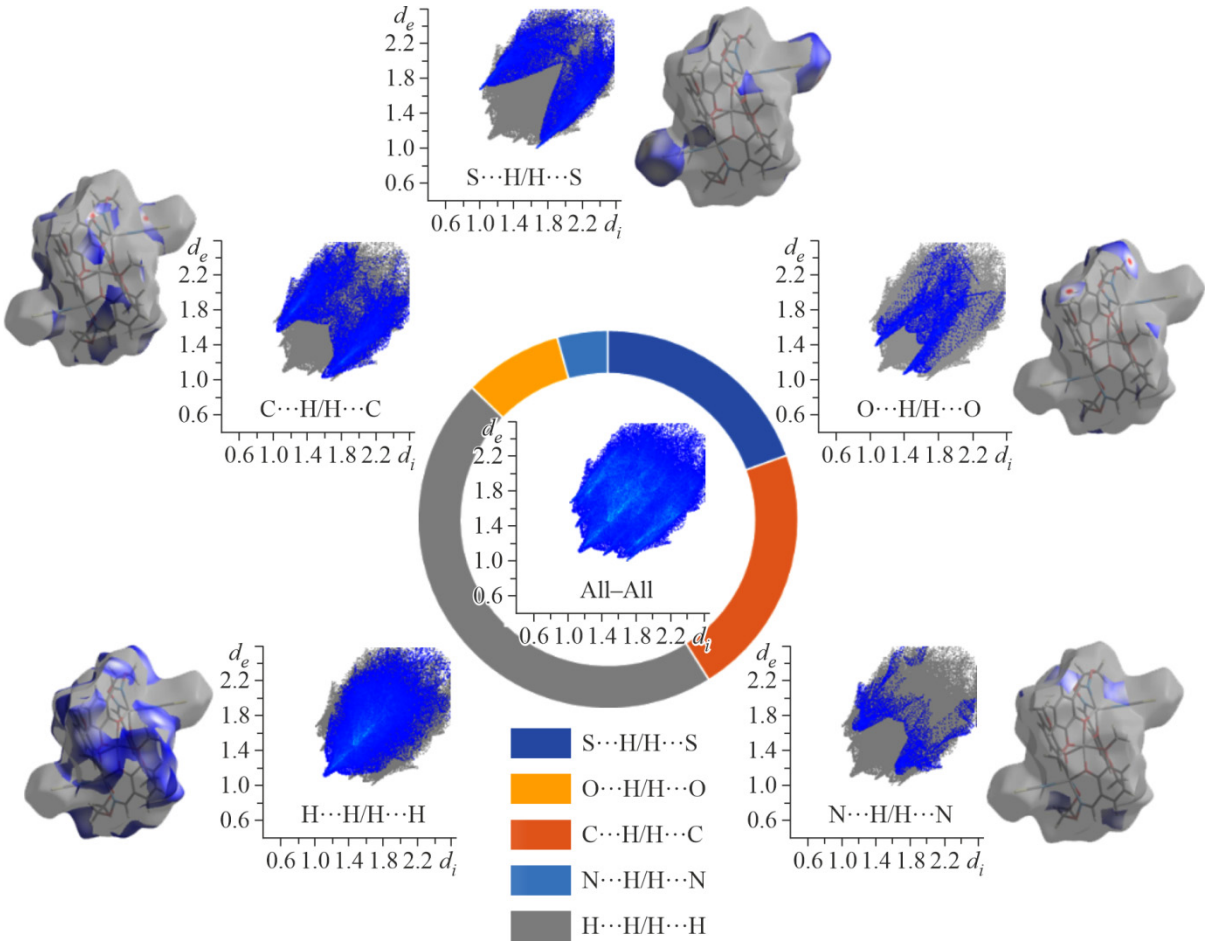

Fig. 7. Fingerprint plots: All (middle) and decomposed plots corresponding to all contacts involved in the structure. The relative contributions of various intermolecular contacts to the Hirshfeld surface area of the title structure are displayed by the schematic illustration.

For the Co(II) complex the highest contribution comes from the H···H/H···H interactions (44.1%) which shows the stability of the crystal. At the top left (C–H donor) and bottom right (π acceptor) of the fingerprint plots, there are characteristic "wings" which are identified as a result of C···H (or C–H···π) interactions (20.6%). In the Co(II) complex, due to the existence of co-ligand NCS^- anions, S···H/H···S interactions (18.6%) have the third largest contribution with a wing like structure. The intermolecular O···H/H···O interactions (8.0%) are represented by a pair of distinct spikes in the bottom area of the fingerprint plots.

DFT studies. Density functional theory (DFT) calculations were performed using Gaussian09 [47], Revision D.01 (basis set: B3LYP, Standard basis: SDD). The HOMO and LUMO contour surfaces of the Co(II) complex show the electron distributions between H_2L and Co(II) atoms. As shown in Fig. 8, the electron distribution of the Co(II) complex occurs around the phenoxido oxygen and oxime nitrogen groups of H_2L and NCS^- anions. This means that interaction between Co(II) atoms and H_2L takes place in the N_2O_2 core and NCS^- anions.

In the Co(II) complex, the E_{HOMO} and E_{LUMO} of α spin state in the frontier molecular orbital energy are –4.8381 eV and –2.3742 eV, respectively. The E_{HOMO} and E_{LUMO} of β spin state are –4.8128 eV and –2.2035 eV, respectively. The HOMO–LUMO energy separation can be used to analyze the kinetic stability of molecules [48]. Because the energy is not conducive to the transition of electrons provided in the low-lying HOMO to the high-lying LUMO, the large energy gap value of HOMO–LUMO may be related to high kinetic stability and low chemical reactivity [49, 50]. The ΔE ($\Delta E = E_{LUMO} - E_{HOMO}$) of α and β spin state of the Co(II) complex are 2.4639 eV and 2.6093 eV, respectively. Compared with the previously reported ΔE of ligand H_2L [51], the ΔE of the Co(II) complex is smaller. This shows that the Co(II) complex have good kinetic stability and chemical activity.

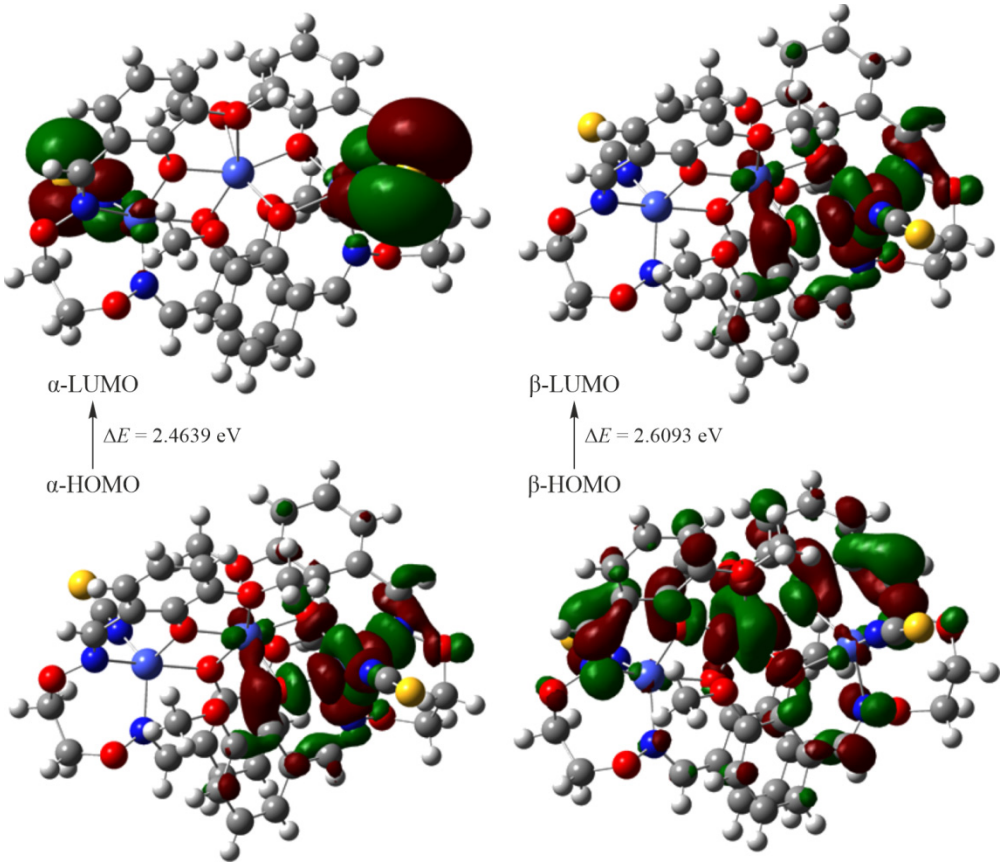

Fig. 8. HOMO–LUMO energy transition diagram of the Co(II) complex.

CONCLUSIONS

To investigate the synthesis, structural characterization, spectroscopic properties, Hirshfeld surface analysis and luminescent properties of the Co(II) complex, first multisite coordinated salamo-based ligand H_2L was prepared. H_2L was then reacted with $Co(OAc)_2{\cdot}4H_2O$ in presence of NCS^- anions in 2:3:2 molar ratios to produce trinuclear Co(II) complexes $[Co_3(L)_2(NCS)_2]$. Investigation of luminescent properties in methanol solution revealed that the Co(II) complex exhibits reduced emission over the ligand H_2L. Apart from, short contacts and different types of supramolecular interactions in the trinuclear Co(II) complex are quantified on the basis of Hirshfeld surface and 2D finger print plot analyses. DFT calculation well confirmed that the Co(II) complex has better kinetic stability and chemical reaction activity than the ligand H_2L.

FUNDING

This work was supported by the National Natural Science Foundation of China (21761018), which is gratefully acknowledged.

CONFLICT OF INTERESTS

The authors declare that they have no conflicts of interests.

REFERENCES

1. P. Mahapatraa, M. G. B. Drewb, and A. Ghosh. *Dalton Trans*., **2020**, *49*, 3372-3374. https://doi.org/10.1039/D0DT90033H
2. T. Feng, L. L. Li, Y. J. Li, and W. K. Dong. *Acta Crystallogr*., *Sect*. *B*, **2021**, *77*, 168-181. https://doi.org/10.1107/s2052520620016157
3. K. Ghosh, K. Harms, A. Bauz, A. Frontera, and S. Chattopadhyay. *Dalton Trans*., **2018**, *47*, 331-347. https://doi.org/10.1039/C7DT03929H
4. D. J. Majumdar, S. Dey, S. S. Sreekumar, S. Das, D. Das, R. K. Metre, K. Bankura, and D. Mishra. *ChemistrySelect*, **2018**, *3*, 12371-12382. https://doi.org/10.1002/slct.201802996
5. E. Tsuchida and K. Oyaizu. *Coord*. *Chem*. *Rev*., **2003**, *237*, 213-228. https://doi.org/10.1016/S0010-8545(02)00251-5
6. C. Adhikary and S. Koner. *Coord*. *Chem*. *Rev*., **2010**, *254*, 2933-2958. https://doi.org/10.1016/j.ccr.2010.06.001
7. K. L. Gurunatha and T. K. Maji. *Inorg*. *Chem*., **2009**, *48*, 10886-10888. https://doi.org/10.1021/ic901804a
8. J. H. He, J. J. Ke, P. H. Chang, K. T. Tsai, P. C. Yang, and I. M. Chan. *Nanoscale*, **2012**, *4*, 3399-3404. https://doi.org/10.1039/C2NR30688C
9. J. Chen, Z. Zhang, Z. Bao, Y. Su, H. Xing, Q. Yang, and Q. Ren. *ACS Appl*. *Mater*. *Interfaces*, **2017**, *9*, 9772-9777. https://doi.org/10.1021/acsami.7b00562
10. M. Strianese, D. Guarnieri, M. Lamberti, A. Landi, A. Peluso, and C. Pellecchia. *Inorg*. *Chem*., **2020**, *59*, 15977-15986. https://doi.org/10.1021/acs.inorgchem.0c02499
11. S. Akine, S. Kagiyama, and T. Nabeshima. *Inorg*. *Chem*., **2010**, *49*, 2141-2152. https://doi.org/10.1021/ic9019926
12. R. N. Bian, X. Xu, T. Feng, and W. K. Dong. *Inorg*. *Chim*. *Acta*, **2021**, *516*, 120098-120108. https://doi.org/10.1016/j.ica.2020.120098
13. J. F. Wang, R. N. Bian, T. Feng, K. F. Xie, L. Wang, and Y. J. Ding. *Microchem*. *J*., **2021**, *160*, 105676-105681. https://doi.org/10.1016/j.microc.2020.105676
14. X. Xu, Y. J. Li, T. Feng, W. K. Dong, and Y. J. Ding. *Luminescence*, **2021**, *36*, 169-179. https://doi.org/10.1002/bio.3932

15. R. N. Bian, J. F. Wang, X. Xu, X. Y. Dong, and Y. J. Ding. *Appl*. *Organomet*. *Chem*., **2021**, *35*, e6040-e6054. https://doi.org/ 10.1002/aoc.6040
16. K. F. Xie, L. L. Li, and W. K. Dong. *J*. *Struct*. *Chem*., **2021**, *62*(6), 876-888. https://doi.org/10.1134/S00224766 2106007X
17. Y. F. Cui, C. Liu, Y. Zhang, and Y. Zhang. *Inorg*. *Nano-Met*. *Chem*., **2021**, *1*, 288-295. https://doi.org/10.1080/ 24701556.2020.1776735
18. R. Kumar, T. Guchhait, V. Subramaniyan, C. Schulzke, and G. Mani. *Dalton Trans*., **2020**, *49*, 13840-13853. https://doi.org/10.1039/D0DT02964E
19. Y. J. Li, S. Z. Guo, T. Feng, K. F. Xie, and W. K. Dong. *J*. *Mol*. *Struct*., **2021**, *1228*, 129796-129806. https://doi.org/ 10.1016/j.molstruc.2020.129796
20. J. F. Wang, X. Xu, R. N. Bian, W. K. Dong, and Y. J. Ding. *Inorg*. *Chim*. *Acta*, **2021**, *516*, 120095-1200105. https://doi.org/10.1016/j.ica.2020.120095
21. Y. H. Deng, Y. J. Yan, J. Zhang, L. P. Na, Y. Zhang, and W. K. Dong. *Inorg*. *Chem*., **2021**, *61*, 1018-1030. https://doi.org/10.1021/acs.inorgchem.1c03066
22. A. Sumiyoshi, Y. Chiba, R. Matsuoka, T. Noda, and T. Nabeshima. *Dalton Trans*., **2019**, *48*, 13169-13175. https://doi.org/10.1039/C9DT02403D
23. J. P. Costes, S. M. Ladeira, L. Vendier, R. Maurice, and W. Wernsdorfer. *Dalton Trans*., **2019**, *48*, 2019-2027. https://doi.org/10.1039/C8DT04716B
24. M. P. Davydova, I. A. Bauer, V. K. Brel, M. I. Rakhmanova, I. Y. Bagryanskaya, and A. V. Artem′ev. *Eur*. *J*. *Inorg*. *Chem*., **2020**, *8*, 695-703. https://doi.org/10.1002/ejic.201901213
25. J. V. Handy, G. Ayala, and R. D. Pike. *Inorg*. *Chim*. *Acta*, **2017**, *456*, 64-75. https://doi.org/10.1016/j.ica.2016.11.013
26. A. V. Artem′ev, M. Z. Shafikov, A. Schinabeck, O. V. Antonova, A. S. Berezin, I. Yu. Bagryanskaya, P. E. Plusnin, and H. Yersin. *Inorg*. *Chem*. *Front*., **2019**, *6*, 3168. https://doi.org/10.1039/C9QI01069F
27. B. Machura, M. Wolff, and J. Palion. *Struct Chem*., **2011**, *22*, 1053-1064. https://doi.org/10.1016/j.poly.2014.04.025
28. J. Boonmak, M. Nakano, N. Chaichit, C. Pakawatchai, and Y. Youngme. *Inorg*. *Chem*., **2011**, *50*, 7324-7333. https://doi.org/10.1021/ic201035c
29. Bruker, APEX2 and SAINT. Madison, WI: Bruker AXS Inc., **2007**.
30. G. M. Sheldrick. SADABS: Program for Empirical Absorption correction of Area Detector Data. Gӧttingen, Germany: University of Gӧttingen, **1996**.
31. O. V. Dolomanov, L. J. Bourhis, R. J. Gildea, J. A. K. Howard, and H. Puschmann. *J*. *Appl*. *Crystallogr*., **2009**, *42*, 339-341. https://doi.org/10.1107/S0021889808042726
32. Y. Zhang, L. L. Li, S. S. Feng, T. Feng, and W. K. Dong. *Russ*. *J*. *Gen*. *Chem*., **2021**, *91*, 2069-2078. https://doi.org/ 10.1134/S1070363221100248
33. P. Li, G. X. Yao, M. Li, and W. K. Dong. *Polyhedron*, **2021**, *195*, 114981-114992. https://doi.org/10.1016/j.poly.2020. 114981
34. X. Xu, T. Feng, S. S. Feng, and W. K. Dong. *Appl*. *Organomet*. *Chem*., **2021**, *35*, e6057-e6070. https://doi.org/10.1016/ 10.1002/aoc.6057
35. J. F. Wang, T. Feng, Y. J. Li, Y. X. Sun, W. K. Dong, and Y. J. Ding. *J*. *Mol*. *Struct*., **2021**, *1231*, 129950-129964. https://doi.org/10.1016/j.molstruc.2021.129950
36. S. Z. Zhang, G. Guo, W. M. Ding, J. Li, Y. Wu, H. J. Zhang, J. Q. Guo, and Y. X. Sun. *J*. *Mol*. *Struct*., **2021**, *1230*, 129627-12635. https://doi.org/10.1016/j.molstruc.2020.129627
37. Y. D. Peng, R. Y. Li, P. Li, and Y. X. Sun. *Crystals*, **2021**, *11*, 113-124. https://doi.org/10.3390/cryst11020113
38. S. Dietmar. *J*. *Organomet*. *Chem*., **1978**, *156*, C47/C48. https://doi.org/10.1016/S0022-328X(00)93553-8
39. Y. Zhang, M. Yu, Y. Q. Pan, Y. Zhang, L. Xu, and X. Y. Dong. *Appl*. *Organomet*. *Chem*., **2020**, *34*, e5442-e5455. https://doi.org/10.1002/aoc.5442

40. S. Akine and T. Nabeshima. *Heteroatom Chem*., **2014**, *25*, 410-421. https://doi.org/10.1002/hc.21205
41. X. X. An, C. Liu, Z. Z. Chen, K. F. Xie, and W. K. Dong. *Crystals*, **2019**, *9*, 602-617. https://doi.org/10.3390/cryst9110602
42. D. Pugliese, N. G. Boetti, J. Lousteau, E. C. Ginistrelli, E. Bertone, F. Geobaldo, and D. Milanese. *J. Alloys Compd*., **2016**, *657*, 678-683. https://doi.org/10.1016/j.jallcom.2015.10.126
43. Y. Zhang, Y. Q. Pan, M. Yu, X. Xu, and W. K. Dong. *Appl. Organomet. Chem*., **2019**, *33*, e5240. https://doi.org/10.1002/aoc.5240
44. M. A. Spackman and D. Jayatilaka. *CrystEngComm*, **2009**, *11*, 19-32. https://doi.org/10.1039/B818330A
45. J. J. McKinnon, D. Jayatilaka, and M. A. Spackman. *Chem. Commun*., **2007**, *37*, 3814. https://doi.org/10.1039/B107147P
46. P. R. Spackman, M. J. Turner, J. J. McKinnon, S. K. Wolff, D. J. Grimwood, D. Jayatilaka, and M. A. Spackman. *J. Appl. Crystallogr*., **2021**, *54*, 1006-1011. https://doi.org/10.1107/S1600576721002910
47. M. A. Spackman and J. J. McKinnon. *CrystEngComm*, **2002**, *66*, 378-392. https://doi.org/10.1039/B203191B
48. M. J. Frisch, G. W. Trucks, H. B. Schlegel, G. E. Scuseria, M. A. Robb, J. R. Cheeseman, G. Scalmani, V. Barone, B. Mennucci, G. A. Petersson, H. Nakatsuji, M. Caricato, X. Li, H. P. Hratchian, A. F. Izmaylov, J. Bloino, G. Zheng, J. L. Sonnenberg, M. Hada, M. Ehara, K. Toyota, R. Fukuda, J. Hasegawa, M. Ishida, T. Nakajima, Y. Honda, O. Kitao, H. Nakai, T. Vreven, J. A. Montgomery Jr., J. E. Peralta, F. Ogliaro, M. Bearpark, J. J. Heyd, E. Brothers, K. N. Kudin, V. N. Staroverov, R. Kobayashi, J. Normand, K. Raghavachari, A. Rendell, J. C. Burant, S. S. Iyengar, J. Tomasi, M. Cossi, N. Rega, J. M. Millam, M. Klene, J. E. Knox, J. B. Cross, V. Bakken, C. Adamo, J. Jaramillo, R. Gomperts, R. E. Stratmann, O. Yazyev, A. J. Austin, R. Cammi, C. Pomelli, J. W. Ochterski, R. L. Martin, K. Morokuma, V. G. Zakrzewski, G. A. Voth, P. Salvador, J. J. Dannenberg, S. Dapprich, A. D. Daniels, O. Farkas, J. B. Foresman, J. V. Ortiz, J. Cioslowski, and D. J. Fox. Gaussian09, Revision A.1. Wallingford CT: Gaussian Inc., **2009**.
49. K. Kim and Y. K. Han. *Theor. Chem. Acc*., **2005**, *113*, 233-237. https://doi.org/10.1007/s00214-005-0630-7
50. J. Aihara. *J. Phys. Chem. A*, **1999**, *103*, 7487-7495. https://doi.org/10.1021/jp990092i
51. Y. Zhang, L. L. Li, S. S. Feng, and W. K. Dong. *Russ. J. Gen. Chem*., **2021**, *91*, 2069-2078. https://doi.org/10.1134/S1070363221100248